Applied and Computational Mathematics
2014; 3(2): 48-56
Published online April 30, 2014 (http://www.sciencepublishinggroup.com/j/acm)
doi: 10.11648/j.acm.20140302.12

Effect of variable thermal conductivity on heat and mass transfer flow over a vertical channel with magnetic field intensity

Ime Jimmy Uwanta, Halima Usman

Department of Mathematics, Usmanu Danfodiyo University, Sokoto, Nigeria

Email address:
imeuwanta@yahoo.com(I. J. Uwanta), hhalimausman@yahoo.com (H. Usman)

To cite this article:
Ime Jimmy Uwanta, Halima Usman. Effect of Variable Thermal Conductivity on Heat and Mass Transfer Flow over a Vertical Channel with Magnetic Field Intensity. *Applied and Computational Mathematics.* Vol. 3, No. 2, 2014, pp. 48-56.
doi: 10.11648/j.acm.20140302.12

Abstract: The objective of this paper is to study thermal conductivity and magnetic field intensity effects on heat and mass transfer flow over a vertical channel both numerically and analytically. The non-linear partial differential equations governing the flow are non-dimensionalised, simplified and solved using Crank Nicolson type of implicit finite difference method. To check the accuracy of the numerical solution, steady state solutions for velocity, temperature and concentration fields are obtained by using perturbation method. Graphical results for velocity, temperature, concentration, skin friction, Nusselt number and Sherwood number have been obtained, to show the effects of different parameters entering in the problem. Results from these study shows that velocity, temperature and concentration increases with the increase in the dimensionless time until they reach steady state value. Also, it was observed that the analytical and numerical solutions agree very well at large values of time.

Keywords: Thermal Conductivity, Heat and Mass Transfer, Magnetic Field, Thermal Radiation

1. Introduction

The influence of magnetic field intensity and thermal conductivity on the study of heat and mass transfer flow over a vertical channel is currently attracting the attention of a growing number of researchers because of their immense potential use in science, technology and engineering applications. The effect of magnetic field on viscous incompressible flow of electrically conducting fluid has its importance in many applications such as metallurgical processes which involves the cooling of filaments, in the fields of stellar and planetary magneto spheres, aeronautics, plasma physics, nuclear science etc. Magnetic field intensity also plays important role in agriculture, petroleum industries, geological formations, thermal recovery of oil and many other places that are important for our industrial and financial developments. In most of the studies on hydromagnetic heat and mass transfer, thermal conductivity has been taken as constant. In metallurgical engineering processing, the thermal conductivity is in fact temperature dependent. That is the numerical value of thermal conductivity changes with temperature. Therefore to predict the flow of heat and mass transfer accurately, mathematical models must consider the variation of thermal conductivity with temperature. Comprehensive reviews on the subject to the above problems have been made by Evans [6] and Sparrow et al. [17]. Many researchers have studied the effects of thermal conductivity and magnetic field intensity on free convection flow of heat and mass transfer.

Cheng [4] studied the effect of magnetic field on heat and mass transfer by natural convection from a vertical surface in porous medium. Venkateswalu et al. [19] investigated finite difference analysis on convective heat transfer flow through a porous medium in a vertical channel with magnetic field. Sharma and Singh [16] have discussed in detail the effect of variable thermal conductivity in MHD fluid flow over a stretching sheet considering heat source and sink parameter. In another article, Mahmoud [8] studied the effect of variable thermal conductivity and radiation on the micropolar fluid flow in the presence of a transverse magnetic field. Noreen et al. [9] have presented a mathematical model investigating the mixed convective heat and mass transfer effects on peristaltic flow of magneto hydrodynamic pseudo plastic

fluid in a symmetric channel. Additionally, Zhang and Huang [20] described the effect of local magnetic field on electrically conducting fluid flow and heat transfer. Also, work on the effect of variable viscosity and thermal conductivity of micropolar fluid in a porous channel in presence of magnetic field has been developed by Patowary [12]. Similarly, Seddek et al. [15] studied the effects of temperature dependent viscosity and thermal conductivity on unsteady MHD convective heat transfer past a semi-infinite vertical porous plate taking into account the effect of a magnetic field in the presence of variable suction.

Elbashbeshy et al. [5] have presented a theoretical study on the effect of magnetic field on flow and heat transfer over a stretching horizontal cylinder in the presence of a heat source/sink with suction/injection. Ahmed [1] analyzed a mathematical model of induced magnetic field with viscous/magnetic dissipation bounded by a porous vertical plate in the presence of radiation. Salem [14] investigated variable viscosity and thermal conductivity effects on MHD flow and heat transfer in visco elastic fluid over a stretching sheet. In another article, a steady two-dimensional magneto hydrodynamic heat and mass transfer free convection flow along a vertical stretching sheet in the presence of magnetic field has been examined by Hosain and Samand [7]. A numerical investigation on the study of the effect of thermal conductivity on MHD flow past an infinite vertical plate with Soret and Dufour effects has been carried out by Usman and Uwanta [18]. Parvin [11] presented a review of magneto hydrodynamic flow heat and mass transfer characteristics in a fluid. In a related development, Oahimire and Olajuwon [10] described the study of hydro magnetic flow of a viscous fluid near a stagnation point on a linearly stretching sheet with variable thermal conductivity and heat source. Recently, Qasim et al. [13] have considered MHD boundary layer slip flow and heat transfer of Ferro fluid along a stretching cylinder with prescribed heat flux. Most recently, Azizian et al. [2] investigated the effect of magnetic field on laminar convective heat transfer of magnetic nano fluids.

In spite of all these studies, the present investigation focuses on the effect of thermal conductivity on heat and mass transfer flow over a vertical channel taking into account the induced magnetic field intensity. The present study may have useful applications to several transport processes as well as magnetic material processing.

2. Mathematical Formulation

Consider an unsteady flow of a viscous incompressible fluid past a vertical channel with variable thermal conductivity and magnetic field intensity. A magnetic field B_0 of uniform strength is applied transversely to the direction of the flow. The $x'-$axis is taken along the plate in the vertically upward direction and the $y'-$ axis is normal to the plate in the direction of the applied uniform magnetic field. The fluid being electrically conducting, the magnetic Reynolds number is assumed to be very small and hence the induced magnetic field can be neglected in comparison with the applied magnetic field in the absence of any input electric field. It is also assumed that the effect of viscous dissipation is negligible in the energy equation. Under the above assumptions as well as the Boussinesq's approximation, the equations of conservation of mass, momentum, energy and species governing the free convection boundary layer flow past a vertical channel can be expressed as:

$$\frac{\partial v'}{\partial y'}=0 \tag{1}$$

$$\frac{\partial u'}{\partial t'}=\nu\frac{\partial^2 u'}{\partial y'^2}-\frac{\sigma B_0^2}{\rho}u'-\frac{\nu}{k^*}u'+g\beta\left(T'-T_0'\right)+g\beta^*\left(C'-C_0'\right) \tag{2}$$

$$\frac{\partial T'}{\partial t'}=\frac{k_0}{\rho C_p}\frac{\partial}{\partial y'}\left[1+\alpha\left(T'-T_0'\right)\frac{\partial T'}{\partial y'}\right]-\frac{1}{\rho C_p}\frac{\partial q_r}{\partial y'} \tag{3}$$

$$\frac{\partial C'}{\partial t'}=D\frac{\partial^2 C'}{\partial y'^2}-R^*\left(C'-C_0'\right) \tag{4}$$

with the following initial and boundary conditions as follows:

$$t\le 0,\ u'=0, T'\to T_w', C'\to C_w' \text{ for all } y'$$

$$\text{t}>0,\ u'=0, T'=T_w', C'=C_w' \text{ at } y'=0$$

$$u'=0, T'=T_0, C'=C_0 \text{ at } y'=H \tag{5}$$

The thermal radiation is assumed to be present in the form of a unidirectional flux in the $y-$ direction that is transverse to the vertical surface. Using the Rosseland approximation by Brewster [3] the radiative heat flux q_r is given by:

$$q_r=-\frac{4\sigma_0'}{3k'}\frac{\partial T'^4}{\partial y'} \tag{6}$$

where u' and v' are the Darcian velocity components in the x and y directions respectively, t is the time, ν is the kinematic viscosity, g is the acceleration due to gravity, β is the coefficient of volume expansion with temperature, ρ is the density of the fluid, σ is the scalar electrical conductivity, β^* is the volumetric coefficient of expansion with concentration, C_p is the specific heat capacity at constant pressure, k^* is the dimensionless permeability of the porous medium, k_0 is the dimensionless thermal conductivity of the ambient fluid, α is a constant

depending on the nature of the fluid, R^* is the dimensionless chemical reaction, D is the coefficient of molecular diffusivity, B_0 is the magnetic induction of constant strength, q_r is the radiative heat flux in the $y-$direction, $\sigma_0^{'}$ is the Stefan-Boltzmann constant, $k^{'}$ is the mean absorption coefficient, $T^{'}$ and $T_0^{'}$ are the temperatures of the fluid inside the thermal boundary layer and the fluid temperature in the free stream respectively, while $C^{'}$ and $C_0^{'}$ are the corresponding concentrations.

To obtain the solutions of equations (2), (3) and (4) subject to the conditions (5) in non-dimensional forms, we introduce the following non-dimensional quantities:

$$
\begin{aligned}
&u=\frac{u^{'}}{u_0}, t=\frac{t^{'}u_0}{H^2}, y=\frac{y^{'}}{H}, \theta=\frac{T^{'}-T_0^{'}}{T_w^{'}-T_0^{'}}\\
&, C=\frac{C^{'}-C_0^{'}}{C_w^{'}-C_0^{'}}, \Pr=\frac{u_0\rho C_p}{k_0}, M=\frac{\sigma B_0^2H^2}{\rho u_0},\\
&Sc=\frac{u_0}{D}, k=\frac{k^*u_0}{\nu H^2}, K_r=\frac{R^*H^2}{u_0},\\
&\lambda=\alpha\left(T^{'}-T_0^{'}\right), R=\frac{16a\sigma_0^{'}HT_0^{'3}}{k^{'}u_0^2},\\
&Gr=\frac{H^2g\beta\left(T_w^{'}-T_0^{'}\right)}{u_0^2},\\
&Gc=\frac{H^2g\beta^*\left(C_w^{'}-C_0^{'}\right)}{u_0^2}.
\end{aligned}
\tag{7}
$$

Applying these non-dimensionless quantities (7), the set of equations (2), (3), (4), and (5) reduces to the following:

$$
\begin{aligned}
&\frac{\partial u}{\partial t}=\frac{\partial^2u}{\partial y^2}-Mu-\frac{1}{k}u+\\
&Gr\theta+GcC
\end{aligned}
\tag{8}
$$

$$
\begin{aligned}
&\Pr\frac{\partial\theta}{\partial t}=(1+\lambda\theta)\frac{\partial^2\theta}{\partial y^2}+\\
&\lambda\left(\frac{\partial\theta}{\partial y}\right)^2-R\theta
\end{aligned}
\tag{9}
$$

$$
\frac{\partial C}{\partial t}=\frac{1}{Sc}\frac{\partial^2C}{\partial y^2}-K_rC \tag{10}
$$

The initial and boundary conditions in non-dimensional quantities are:

$$
\begin{aligned}
&t\le 0,\ u=0,\theta=,C=0 \text{ for all } y\\
&\text{t} > 0,\ u=0,\theta=1,C=1 \text{ at } y=0\\
&u=0,\theta=0,C=0 \text{ at } y=1
\end{aligned}
\tag{11}
$$

where M is the magnetic field parameter, k is the porous parameter, Gr is the thermal Grashof number, Gc is the solutal Grashof number, Pr is the Prandtl number, λ is the variable thermal conductivity parameter, R is the radiation parameter, K_r is the chemical reaction parameter, Sc is the Schmidt number, t is the dimensionless time, while u and v are the dimensionless velocity components in $x-$ and $y-$ directions respectively.

The skin friction, Nusselt number and Sherwood number are the important physical parameters for this type of boundary layer flow, which in non- dimensional form respectively are given by:

The skin-friction coefficient, Nusselt number and Sherwood number are the important physical parameters for this type of boundary layer flow, which in non-dimensional form respectively are given by:

$$
C_f=\left(\frac{\partial u}{\partial y}\right)_{y=0}, Nu=-\left(\frac{\partial\theta}{\partial y}\right)_{y=0}, Sh=\left(\frac{\partial C}{\partial y}\right)_{y=0} \tag{12}
$$

3. Analytical Solutions

The governing equations presented in this problem are highly coupled and non linear and exhibit no closed-form solutions. In order to check the accuracy of the present numerical scheme of this model, there is need to compare numerical solutions with the analytical solutions. Since the governing equations are non-linear, it is, therefore, of interest to reduce the governing equations of the present problem to a form that can be solved in closed form. At steady state the physical parameters do not have any effect, hence the steady state equations and boundary conditions for the problem can be written as

$$
\frac{\partial^2u}{\partial y^2}-\left(M+\frac{1}{k}\right)u+Gr\theta+Gc=0 \tag{13}
$$

$$
\frac{\partial^2\theta}{\partial y^2}-R\theta=0 \tag{14}
$$

$$
\frac{\partial^2C}{\partial y^2}-ScK_r=0 \tag{15}
$$

The boundary conditions are:

$$
\begin{aligned}
&u=0,\ \theta=1,\ C=1,\ \ at\ y=0,\\
&u=0,\ \theta=0,\ C=0\ \ at\ y=1.
\end{aligned}
\tag{16}
$$

To find the approximate solution to equations (13)-(15) subject to equation (16), we use perturbation method, which is a method that is used to approximate the solution to a differential equation analytically. Therefore the physical variables u, θ and C can be expanded in the power of $(R<<1)$. This can be possible physically as R for the flow is always less than unity. Hence we can assume solution of the form

$$\begin{aligned} u &= u_0(y) + Ru_1(y) + 0(R^2) \\ \theta &= \theta_0(y) + R\theta_1(y) + 0(R^2) \\ C &= C_0(y) + RC_1(y) + 0(R^2) \end{aligned} \tag{17}$$

Using equation (17) in equations (13)-(16) and equating the coefficient of like powers of R, we have:

$$u_0'' - \left(M + \frac{1}{k}\right)u_0 = -Gr\theta_0 + GcC_0 \tag{18}$$

$$\theta_0'' = 0 \tag{19}$$

$$C_0'' - ScK_rC_0 = 0 \tag{20}$$

$$u_1'' - \left(M + \frac{1}{k}\right)u_1 = -Gr\theta_1 - GcC_1 \tag{21}$$

$$\theta_1'' = \theta_0 \tag{22}$$

$$C_1'' - ScK_rC_1 = 0 \tag{23}$$

The corresponding boundary conditions are

$$\begin{aligned} &u_0 = 0, \quad \theta_0 = 1, \quad C_0 = 1 \\ &u_1 = 0, \quad \theta_1 = 0, \quad C_1 = 0 \qquad at \quad y = 0 \\ &u_0 = 0, \quad \theta_0 = 0, \quad C_0 = 0 \\ &u_1 = 0, \quad \theta_1 = 0, \quad C_1 = 0 \qquad at \quad y = 1 \end{aligned} \tag{24}$$

Solving equations (18)-(23) with the help of equation (24), we get:

$$\begin{aligned} u_0 &= H_1e^{y\sqrt{p}} + H_2e^{-y\sqrt{p}} + E_1 + \\ &E_2y + E_3e^{y\sqrt{ScK_r}} + E_4e^{-y\sqrt{ScK_r}} \end{aligned} \tag{25}$$

$$\theta_0 = 1 - y \tag{26}$$

$$C_0 = Ae^{y\sqrt{ScK_r}} + Be^{-y\sqrt{ScK_r}} \tag{27}$$

$$\begin{aligned} u_1 &= H_3e^{y\sqrt{p}} + H_4e^{-y\sqrt{p}} + E_5y^3 + \\ &E_6y^2 + E_7y + E_8 \end{aligned} \tag{28}$$

$$\theta_1 = -\frac{1}{3}y + \frac{1}{2}y^2 - \frac{1}{6}y^3 \tag{29}$$

$$C_1 = 0 \tag{30}$$

In view of the above equations the solutions are:

$$\begin{aligned} u &= H_1e^{y\sqrt{p}} + H_2e^{-y\sqrt{p}} + E_1 + E_2y + \\ &E_3e^{y\sqrt{ScK_r}} + E_4e^{-y\sqrt{ScK_r}} + \\ &R\left(H_3e^{y\sqrt{p}} + H_4e^{-y\sqrt{p}} + E_5y^3 + E_6y^2 + E_7y + E_8\right) \end{aligned} \tag{31}$$

$$\theta = 1 - y + R\left(-\frac{1}{3}y + \frac{1}{2}y^2 - \frac{1}{6}y^3\right) \tag{32}$$

$$C = Ae^{y\sqrt{ScK_r}} + Be^{-y\sqrt{ScK_r}} \tag{33}$$

4. Numerical Solution Procedure

In order to solve the unsteady non-linear coupled partial differential equations (8)-(10) with the associated initial and boundary conditions (11), an implicit finite difference technique of Crank-Nicolson type which is known to converge rapidly and unconditionally stable has been employed. The finite difference equations corresponding to equations (8)-(10) using the method are as follows:

$$\begin{aligned} &\frac{u_i^{j+1} - u_i^j}{\Delta t} = \frac{1}{2(\Delta y)^2} \\ &\left(u_{i+1}^{j+1} - 2u_i^{j+1} + u_{i-1}^{j+1} + u_{i+1}^j - 2u_i^j + u_{i-1}^j\right) - \\ &Mu_i^j - \frac{1}{k}u_i^j + Gr\theta_i^j + GcC_i^j \end{aligned} \tag{34}$$

$$\begin{aligned} &\Pr\left(\frac{\theta_i^{j+1} - \theta_i^j}{\Delta t}\right) = \frac{H}{2(\Delta y)^2} \\ &\left(\theta_{i+1}^{j+1} - 2\theta_i^{j+1} + \theta_{i-1}^{j+1} + \theta_{i+1}^j - 2\theta_i^j + \theta_{i-1}^j\right) + \\ &\frac{\lambda}{(\Delta y)^2}\left(\theta_{i+1}^j - \theta_i^j\right)^2 - R\theta_i^j \end{aligned} \tag{35}$$

$$\begin{aligned} &\frac{C_i^{j+1} - C_i^j}{\Delta t} = \frac{1}{2Sc(\Delta y)^2} \\ &\left(C_{i+1}^{j+1} - 2C_i^{j+1} + C_{i-1}^{j+1} + C_{i+1}^j - 2C_i^j + C_{i-1}^j\right) - \\ &K_rC_i^j \end{aligned} \tag{36}$$

The initial and boundary conditions may be expressed as

$$\begin{aligned} &u_{i,j} = 0, \quad \theta_{i,j} = 0, \quad C_{i,j} = 0 \\ &u_{0,j} = 0, \quad \theta_{0,j} = 1, \quad C_{0,j} = 1 \\ &u_{H,j} = 0, \quad \theta_{H,j} = 0, \quad C_{H,j} = 0 \end{aligned} \tag{37}$$

where H corresponds to 1.

Equations (34), (35) and (36) may be written respectively as follows:

$$\begin{aligned} &-d_1u_{i-1}^{j+1} + d_2u_i^{j+1} - d_1u_{i+1}^{j+1} = d_1u_{i-1}^j + \\ &\left(d_3 - d_4\right)u_i^j + d_1u_{i+1}^j + d_5\theta_i^j + d_6C_i^j \end{aligned} \tag{38}$$

$$\begin{aligned} &-d_7\theta_{i-1}^{j+1} + d_8\theta_i^{j+1} - d_7\theta_{i+1}^{j+1} = d_7\theta_{i-1}^j + \\ &d_9\theta_i^j + d_7\theta_{i+1}^j + d_{10}\left(\theta_{i+1}^j - \theta_i^j\right)^2 - d_{11}\theta_i^j \end{aligned} \tag{39}$$

$$\begin{aligned} &-d_{12}C_{i-1}^{j+1} + d_{13}C_i^{j+1} - d_{12}C_{i+1}^{j+1} = d_{12}C_{i-1}^j + \\ &\left(d_{14} - d_{15}\right)C_i^j + d_{12}C_{i+1}^j \end{aligned} \tag{40}$$

The index i corresponds to space y and j corresponds to

time t. Δy and Δt are the mesh sizes along y-direction and time t-direction respectively. The finite difference equations (38)-(40) at every internal nodal point on a particular n-level constitute a tri-diagonal system of equations, which are solved by using the Thomas algorithm.

In each time step, the temperature and concentration profiles have been computed first from equations (39) and (40) and then the computed values are used to obtain the velocity profile at the end of time steps that is $u_{i,j+1}$ computed from equation (38). This process is carried out until the steady state is reached. The steady-state solution of the convergence criteria for stability of the scheme is assumed to have been reached, when the absolute differences between the values of velocity, temperature and concentration at two consecutive time steps are less than 10^{-5} at all grid points. Computations are carried out for different values of physical parameters involved in the problem.

5. Results and Discussion

In order to report on the analysis of the fluid flow, numerical computations are carried out for various values of magnetic parameter (M), thermal Grashof number (Gr), solutal Grashof number (Gc), permeability parameter (k), thermal conductivity parameter (λ), radiation parameter (R), Prandtl number (Pr), Schmidt number (Sc), chemical reaction parameter (K_r) and dimensionless time (t). Therefore, this study is focused on the effects of these governing parameters on the transient velocity, temperature as well as concentration profiles. Here, the main discussion is restricted to the aiding of favourable case only, for fluids with Prandtl number ($Pr = 0.71, 1.0, 3.0, 7.0$) that represent air, atmospheric pressure, Freon and water respectively. The diffusing chemical species of most common interest in air has Schmidt number and is taken for water ($Sc = 0.60$), Carbon dioxide ($Sc = 0.94$), Methanol ($Sc = 1.0$) and Propyl benzene ($Sc = 2.62$). The value of thermal Grashof number is taken to be positive which correspond to the cooling of the plate.

The default values of the thermo physical parameters are specified as follows:

$$Gr = 5, Gc = 5, M = 2, \mathrm{Pr} = 0.71, k = 0.5,$$
$$R = 5, \lambda = 0.5, K_r = 1, Sc = 0.60$$

All graphs therefore correspond to these values unless otherwise indicated.

Figures (1) and (2) illustrate the influence of thermal Grashof number Gr in case of cooling of the plate and the solutal Grashof number Gc. It is noticed that an increase in Gr and Gc results in an increase in the velocity. It is due to the fact that increase in the values of Gr and Gc has the tendency to increase the thermal and mass buoyancy effect. This gives rise to an increase in the induced flow. In figure (3) it is observed that increasing permeability parameter k enhances the velocity of the fluid. The effect of magnetic field parameter M in case of cooling the plate on the velocity profile is depicted in figure (4). It is found that the velocity decreases with increasing magnetic parameter. The effect of radiation parameter R on the temperature variation for two working fluids air ($\mathrm{Pr} = 0.71$) and water ($\mathrm{Pr} = 7.0$) is graphically illustrated in figure (5). It is evident from this figure that as R increases, considerable reduction is observed in temperature profiles. Figure (6) reveals the transient temperature profiles against y (distance from the plate) for different values of thermal conductivity parameter ($\lambda = V$) in case of air ($\mathrm{Pr} = 0.71$) and water ($\mathrm{Pr} = 7.0$). It is seen that as λ increases for both air and water, the temperature increases which is physically true because thermal conductivity of fluid increases with increasing Prandtl number, resulting in thermal boundary layer thickness thereby increasing the temperature profiles.

Figures (7) and (8) describe the behavior of concentration profiles for different values of Schmidt number Sc and chemical reaction parameter K_r. A decrease in concentration with increasing Sc as well as K_r is observed from these figures. Also, it is noted that the concentration boundary layer becomes thin as the Schmidt number as well as the chemical reaction parameter increases. Figures (9-11) show the velocity distribution, temperature and concentration profiles with variation of dimensionless time t respectively. It can be seen that the velocity, temperature and concentration of the fluid increases with time and ultimately reaches their steady state values for air ($\mathrm{Pr} = 0.71$).

The validity of the present model has been verified by comparing the numerical solutions and the analytical solutions through figures (12)-(14) for velocity, temperature and concentration profiles respectively. These results are presented to illustrate the accuracy of the numerical solution. It is observed that the agreement between the results is good because the curves corresponding to analytical and numerical solutions are lying close to the other. This has established confidence in the numerical results reported in this paper.

Figure (15) shows the variation of skin friction coefficient against magnetic parameter M for different values of thermal Grashof number Gr, solutal Grashof number Gc and permeability parameter k. It depicts that the skin friction increases with an increase in any of these parameters Gr, Gc and k. The effects of Prandtl number Pr and thermal conductivity λ on the Nusselt number against radiation parameter R are presented in figure (16). It is observed that the rate of heat transfer decreases with an increasing Pr. Also, it is found that the rate of heat transfer falls with increasing thermal conductivity. Finally, figure (17) demonstrates the effect of Schmidt number Sc and chemical reaction parameter K_r on Sherwood number. It displays that the rate of concentration transfer increases with increasing values of Sc and K_r.

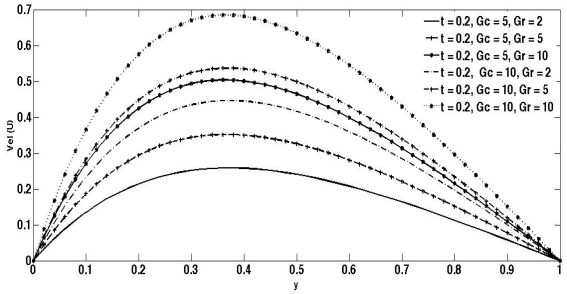

Fig (1). *Velocity profile for different values of thermal Grashof number*

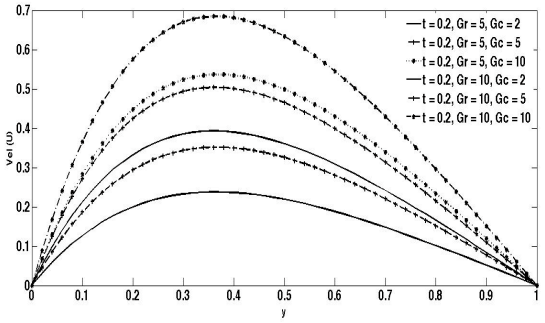

Fig (2). *Velocity profile for different values of solutal Grashof number*

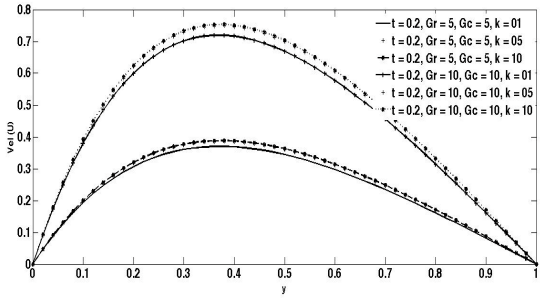

Fig (3). *Velocity profile for different values of porous parameter*

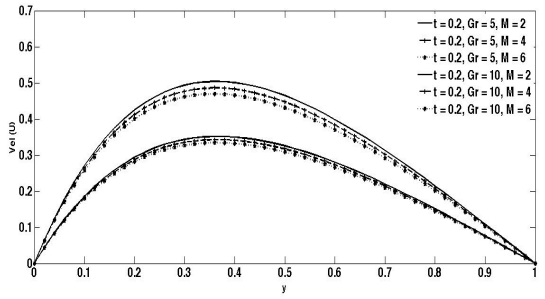

Fig (4). *Velocity profile for different values of magnetic parameter*

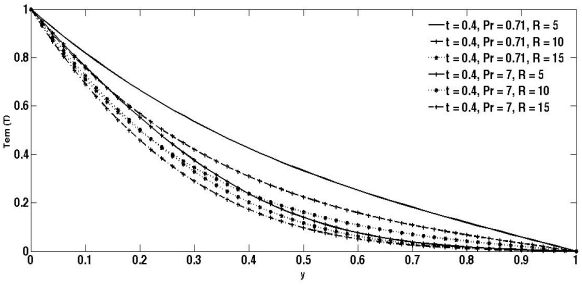

Fig (5). *Temperature profile for different values of radiation parameter*

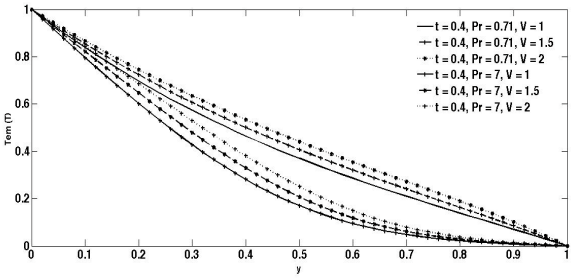

Fig (6). *Temperature profile for different values of variable thermal conductivity*

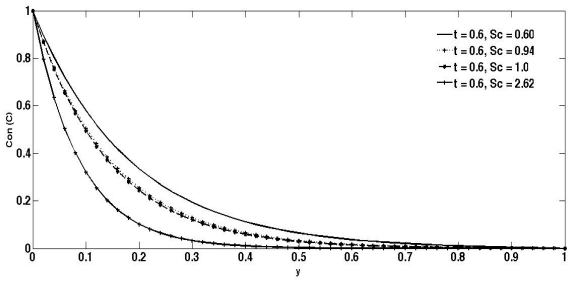

Fig (7). *Concentration profile for different values of Schmidt number*

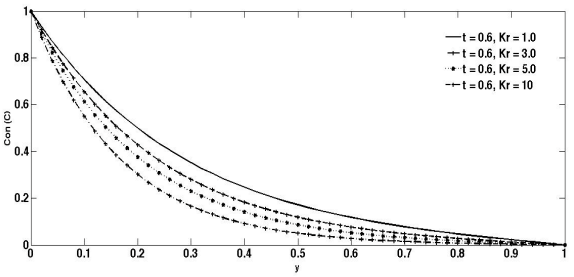

Fig (8). *Concentration profile for different values of chemical reaction parameter*

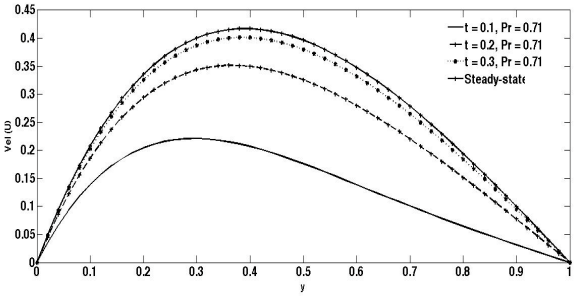

Fig (9). *Velocity profile for different values of dimensionless time*

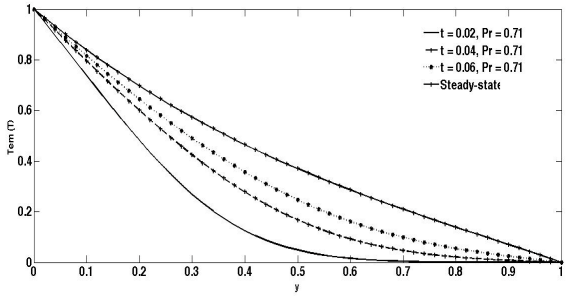

Fig (10). *Temperature profile for different values of dimensionless time*

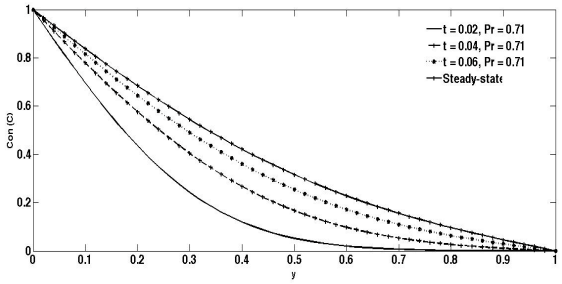

Fig (11). *Concentration profile for different values of dimensionless time*

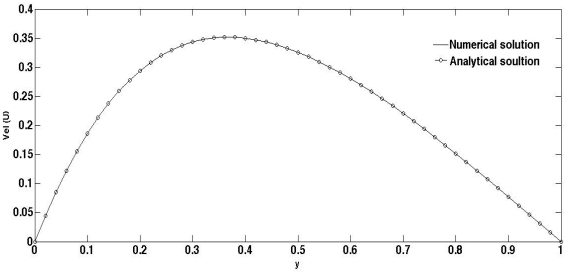

Fig (12). *Comparison of numerical and analytical solutions for velocity profile*

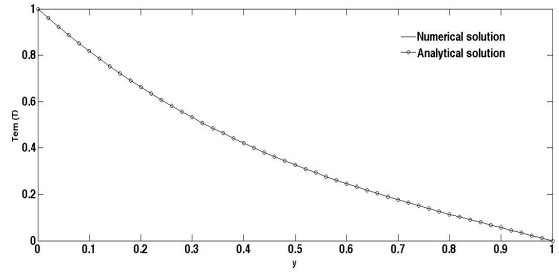

Fig (13). *Comparison of numerical and analytical solutions for Temperature profile*

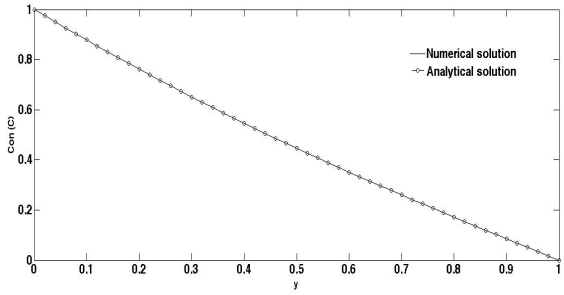

Fig. (14). *Comparison of numerical and analytical solutions for Concentration profile*

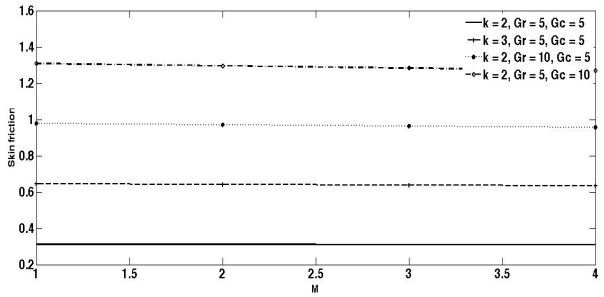

Fig (15). *Skin friction profile for different values of porous parameter, thermal and solutal Grashof numbers*

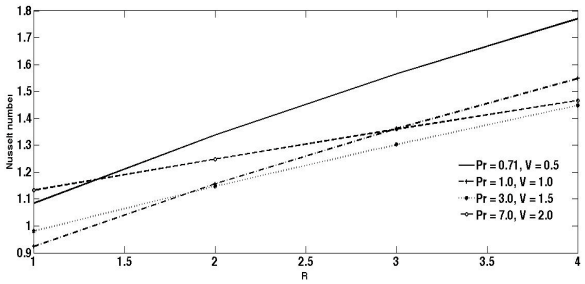

Fig (16). *Nusselt number profile for different values of Prandtl number and variable thermal conductivity*

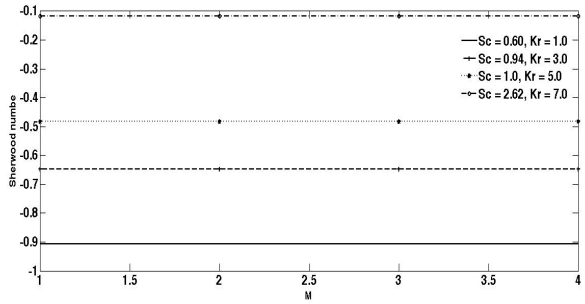

Fig (17). *Sherwood number profile for different values of Schmidt number and chemical reaction parameter*

6. Conclusions

In this paper, the study on the effect of variable thermal conductivity on heat and mass transfer flow over a vertical channel with magnetic field intensity using Crank-Nicolson type of implicit finite difference method has been carried out. The expressions for the velocity, temperature and concentration fields have been constructed and the effects of various parameters on heat and mass transfer characteristics of the fluid flow are discussed graphically. From the present numerical investigation the following conclusions have been drawn:

1. The velocity of the fluid increases with an increase in thermal Grashof number, solutal Grashof number, permeability parameter and dimensionless time, while it decreases with an increase in magnetic field parameter as shown in Figs. (1-4) and Fig. (9.)
2. Increasing thermal conductivity parameter and dimensionless time leads to increase the fluid temperature. This is clearly indicated in Figs. (6) and (10).
3. A decrease in concentration profile with increasing Schmidt number as well as chemical reaction parameter is observed in Figs. (7) and (8).
4. The skin friction coefficient increases with increasing thermal Grashof number, solutal Grashof number and permeability parameter as illustrated in figure (15).
5. The rate of heat transfer in terms of Nusselt number falls with increase in Prandtl number and thermal conductivity parameter is noticed in figure (16).
6. It is marked in figure (17) that the rate of concentration transfer increases with increasing values of Schmidt number and chemical reaction parameter.

7. The accuracy of the present model has been verified by comparing numerical and analytical solutions and the agreement between the results is excellent. This is clearly shown in Figs. (12-14).

The solutions presented in this paper for various thermo physical effects would be useful for subsequent analysis in heat and mass transfer in polymer processing, metallurgical transport modeling and many geophysical processes like crude oil recovery.

Appendix

$$r_1=\frac{\Delta t}{(\Delta y)^2}, r_2=2\Delta tM, r_3=2\Delta tGr, r_4=2\Delta tGc,$$

$$H=1+\lambda\theta, r_5=Hr_1, r_6=2\lambda r_1, r_7=2\Delta tR,$$

$$r_8=2\Delta tScK_r, r_9=2\Delta t\frac{1}{k}, d_1=r_1, d_2=2(1+r_1),$$

$$d_3=2-2r_1-r_9, d_4=r_2, d_5=r_3, d_6=r_4, d_7=r_5,$$

$$d_8=2(\mathrm{Pr}+r_5), d_9=2(\mathrm{Pr}-r_5), d_{10}=r_6, d_{11}=r_7,$$

$$d_{12}=r_1, d_{13}=2(\mathrm{r}_1+Sc), d_{14}=2(Sc-\mathrm{r}_1), d_{15}=r_8,$$

$$A=1-B, B=\frac{-e^{\sqrt{ScK_r}}}{\left(e^{-\sqrt{ScK_r}}-e^{\sqrt{ScK_r}}\right)}, p=\left(M+\frac{1}{k}\right),$$

$$E_1=\frac{Gr}{p}, E_2=-\frac{Gr}{p}, E_3=-\frac{GcA}{ScK_r-p},$$

$$E_4=-\frac{GcB}{ScK_r-p}, E_5=-\frac{Gr}{6p}, E_6=\frac{Gr}{2p},$$

$$E_7=\frac{6E_5}{p}-\frac{Gr}{3p}, E_8=\frac{2E_6}{p},$$

$$H_1=-(H_2+E_1+E_3+E_4),$$

$$H_3=-(H_4+E_8),$$

$$H_2=\frac{1}{\left(e^{-\sqrt{p}}-e^{\sqrt{p}}\right)}\begin{pmatrix}-E_1\left(1-e^{\sqrt{p}}\right)-E_2-E_3\left(e^{\sqrt{ScK_r}}-e^{\sqrt{p}}\right)-\\ E_4\left(e^{-\sqrt{ScK_r}}-e^{\sqrt{p}}\right)\end{pmatrix},$$

$$H_4=\frac{1}{\left(e^{-\sqrt{p}}-e^{\sqrt{p}}\right)}\left(-E_8\left(1-e^{\sqrt{p}}\right)-(E_5+E_6+E_7+E_8)\right).$$

Nomenclature

C – concentration
C_p – specific heat at constant pressure
D - mass diffusivity
g – acceleration due to gravity
Gr – Grashof number
Gc – solutal Grashof number
k – porous parameter
Nu – Nusselt number
Pr – Prandtl number
Sc – Schmidt number
R - radiation parameter
K_r - chemical reaction parameter
T – temperature
C_f -Skin friction
Sh - Sherwood number
u, v – velocities in the x and y-direction respectively
x, y – Cartesian coordinates along the plate and normal to it respectively
B_0 - magnetic field of constant strength
M – magnetic field parameter

Greek Letters

β* - coefficient of expansion with concentration
β - coefficient of thermal expansion
ρ- density of fluid
θ- dimensionless temperature
υ- kinematic viscosity
$\sigma_0^{'}$ - Stefan Boltzmann constant
λ - variable thermal conductivity
σ - electrical conductivity of the fluid

Subscripts

w - condition at wall
∞ - condition at infinity

References

[1] S. Ahmed, "Mathematical model of induced magnetic field with viscous/magnetic dissipation bounded by a porous vertical plate in presence of radiation," International Journal of Applied Mathematics and Mechanics, vol. 8, no.1, pp. 86-104, 2012.

[2] R. Azizian, E. Doroodchi, T. Mckrell, J. Buongiomo, L. W. Hu and B. Moghtaden, "Effect of magnetic field on laminar convective heat transfer of magnetic nano fluids," International Journal of Heat and Mass Transfer, vol. 68, pp. 94-109, 2014.

[3] M. Q. Brewster. Thermal radiative transfer and properties, John Wiley and Sons. Inc, New York, 1992.

[4] C. Y. Cheng, "Effect of magnetic field on heat and mass transfer by natural convection from vertical surfaces in porous media- an integral approach," International Communications in Heat and Mass Transfer, vol. 26, no. 7, pp. 935-943, 1999.

[5] E. M. Elbashbeshy, T. G. Emam, M. S. El-Azaba and K. M. Abdelgaber, "Effect of magnetic field on flow and heat transfer over a stretching horizontal cylinder in the presence of a heat source/sink with suction/ injection," Applied Mechanical Engineering, vol. 1, no. 1, pp. 1-5, 2012.

[6] H. L. Evans, "Mass transfer through laminar boundary layers," International Journal of Heat and Mass Transfer, vol. 5, pp. 35-57, 1962.

[7] M. S. Hosain and M. A. Samad, "Heat and mass transfer of an MHD free convection flow along a stretching sheet with chemical reaction, radiation and heat generation in presence of magnetic field," Research Journal of Mathematics and Statistics, vol. 5, no. 1-2, pp. 5-17, 2013.

[8] M. A. A. Mahmoud, "Thermal radiation effects on MHD flow of a micropolar fluid over a stretching sheet with variable thermal conductivity," Physica A, vol. 375, pp. 401-410, 2007.

[9] S. Noreen, T. Hayat, A. Alsaedi and M. Qasim, "Mixed convection heat and mass transfer in peristaltic flow with chemical reaction and inclined magnetic field," Indian Journal of Physics, vol. 87, no. 9, pp. 889-896, 2013.

[10] J. I. Oahimire and B.I. Olajuwon, "Hydromagnetic flow near a stagnation point on a stretching sheet with variable thermal conductivity and heat source/sink," International Journal of Applied Science and Engineering, vol. 11, no. 3, pp. 331-341, 2013.

[11] K. Parvin, "Review of Magnetohydrodynamic flow heat and mass transfer characteristics in a fluid," International Journal of Science and Research Publications, vol. 3, no. 11, pp. 1-3, 2013.

[12] G. Patowary, "Effect of variable viscosity and thermal conductivity of micropolar fluid in a porous channel in presence of magnetic field," International Journal for Basic Sciences and Social Sciences, vol. 1, no. 3, pp. 69-77, 2012.

[13] M. Qasim, Z. H. Khan, W. A. Khan and I. A. Sha, "MHD boundary layer slip flow and heat transfer of Ferro fluid along a stretching cylinder with prescribed heat flux," PLOS ONE, vol. 9, no. 1, pp. 1-6, 2014.

[14] A. M. Salem, "Variable viscosity and thermal conductivity effects on MHD flow and heat transfer in visco elastic fluid over a stretching sheet," Physics Letters A, vol. 369, no. 4, pp. 315-322, 2007.

[15] M. A. Seddek and F. A. Salema, "The effects of temperature dependent viscosity and thermal conductivity on unsteady MHD convective heat transfer past a semi-infinite vertical porous moving plate with variable suction," Computational Material Sciences, vol. 40, no. 2, pp. 186-192, 2007.

[16] P. R. Sharma and G. Singh, "Effects of variable thermal conductivity and heat source/sink on MHD flow near a stagnation point on a linearly stretching sheet," Journal of Applied Fluid Mechanics, vol. 2, pp. 13-21, 2008.

[17] E. M. Sparrow, E. R. Eckert and W. J. Minkowyez, "Transportation cooling in a magnetohydrodynamic stagnation point flow," Applied Science Research, A, vol. 11, pp. 125-147, 1962.

[18] H. Usman and I. J. Uwanta, "Effect of thermal conductivity on MHD heat and mass transfer flow past an infinite vertical plate with Soret and Dufour effects," American Journal of Applied Mathematics, vol. 1, no. 3, pp. 28-38, 2013.

[19] S. K. Venkateswalu, K. N. Suryanarayana and B. R. Reddy, "Finite difference analysis on convective heat transfer flow through a porous medium in a vertical channel with magnetic field," International Journal of Applied Mathematics and Mechanics, vol. 7, no. 7, pp. 74-94, 2011.

[20] T. Zhang and H. Huang, "Effect of local magnetic field on electrically conducting fluid flow and heat transfer," Journal of heat transfer, vol. 135, no. 2, pp. 1-8, 2012.